Contemporary stress orientations in the Faroe-Shetland region

Simon P. Holford[1], David R. Tassone[1], Martyn S. Stoker[2] & Richard R. Hillis[1,3]

[1]Australian School of Petroleum, University of Adelaide, SA 5005, Australia

[2]British Geological Survey, Murchison House, West Mains Road, Edinburgh, UK

[3]Deep Exploration Technologies Cooperative Research Centre, 26 Butler Boulevard, Burbridge Business Park, Adelaide, SA 5950, Australia

Abstract

The Faroe-Shetland Region (FSR) of the NE Atlantic continental margin contains a number of complexly structured Mesozoic-Palaeogene-age rift basins, but in comparison to the contiguous British Isles and North Sea Basin, the state of crustal stress in the FSR is poorly understood. The orientation of maximum horizontal compressional stress (σ_{Hmax}) across most of NW Europe is ~NW-SE, which is considered to be controlled by forces acting at the plate boundaries. We have determined 16 B-D quality σ_{Hmax} orientations based on borehole breakouts interpreted in petroleum wells, and define three distinct stress provinces within the FSR. Stress orientations in the NE are ~NW-SE, consistent with the regional pattern of stresses in NW Europe and local neotectonic structural trends. However, contemporary stress orientations in the central and SW of the FSR exhibit short-wavelength (distances <10-50 km) variation, with NE-SW, N-S and E-W orientations that are parallel or sub-parallel to underlying structural trends. This variation is interpreted in terms of stress deflections towards weak faults that downthrow the Mesozoic-Cenozoic sedimentary successions against basement highs. These local-scale sources are superposed on a background ~WNW-ESE σ_{Hmax} orientation that is controlled by both plate boundary forces and regional-scale sources of stresses.

Keywords

Contemporary crustal stresses, intraplate stresses, Faroe-Shetland, Atlantic margin, British Isles.

Introduction

The Cenozoic tectonic history of the Faroe-Shetland region (FSR), a complexly structured series of rift basins which includes the Faroe-Shetland Basin (FSB) on the NE Atlantic margin located offshore NW Scotland (Fig. 1), has been the subject of considerable attention in recent years. The Cenozoic sedimentary succession of this basin records a complicated history of vertical motions (Hartley et al., 2011), syn and post-breakup intrusive and extrusive magmatism (Schofield & Jolley, 2013) and compressional deformation and inversion of the basin fill (Stoker et al., 2005), which comprises a substantial component of post-breakup clastic sedimentary input (Stoker et al., 2010). These processes and events have been variously attributed to the activity of the Iceland mantle plume and intraplate shortening controlled by plate boundary forces (e.g. Hillis et al., 2008; Holford et al., 2008, 2009, 2010; Stoker et al., 2010; Hartley et al., 2011; Ellis & Stoker, 2014; Tassone et al., 2014).

Despite the substantial level of interest in the Cenozoic tectonic history of this basin, there is surprisingly little data on its contemporary stress field (Fig. 2). Such data provide valuable constraints on the tectonic controls on this stress field, and also assist oil field development issues such as wellbore instability (Narayanasamy et al., 2010) and production from fractured reservoirs (e.g. the Clair oil field; Ogilvie et al., 2015). Over 160 exploration wells have been drilled in this basin (Austin et al., 2014), but the 2008 release of the World Stress Map (Heidbach et al., 2008) features

maximum horizontal stress (σ_{Hmax}) orientations based on borehole breakouts measured in only three wells by Klein & Barr (1986) (Fig. 2). These three measurements are ranked as B or C-quality using the World Stress Map ranking scheme, and so can be considered as reliable indicators of stress orientations (Zoback, 1992). Two of these measurements (145°N from well 204/28-1, and 130°N from an unidentified well in block 211/12) are broadly consistent with the predominant NW-SE σ_{Hmax} orientation in North West Europe (Müller et al., 1992). However, the measurement from the third well (located in block 202/03 in the North Rona Basin) is characterised by a different σ_{Hmax} orientation of 010°N which hints at the possibility of a variable stress pattern within the basin. Because the available stress measurements are located at opposing ends of this ~400 km long, NW-SE trending basin, there are large areas of this region for which no data are available, and thus stress orientations are unknown.

The paucity of information on crustal stresses in the FSR stands in stark contrast to the quantity of data reported from adjacent regions (Fig. 2). A large number of stress measurements onshore Britain indicate a dominant ~NW-SE σ_{Hmax} orientation (Evans & Brereton, 1990; Baptie, 2010), similar to that observed in other onshore regions surrounding the North Sea such as Germany and the Netherlands (Heidbach et al., 2008). Modelling studies suggest that the intraplate stress field in North West Europe is, to a first order, controlled by plate boundary forces and predict ~NW-SE σ_{Hmax} orientations throughout our study area (Gölke & Coblentz, 1996).

Borehole breakout and earthquake defined σ_{Hmax} orientations in the East Shetland Basin are also ~WNW-ESE (Zanella & Coward, 2003). In the northern North Sea, offshore Norway, σ_{Hmax} orientations based on breakouts and drilling-induced tensile fractures (DITFs) are broadly ~E-W (Grollimund et al., 2001).

Maximum horizontal stress orientations in the central North Sea are highly variable, and generally show no preferred orientation (Hillis & Nelson, 2005). Grollimund et al. (2001) argue that lithosphere flexure caused by deglaciation exerts an important control on the ~E-W σ_{Hmax} orientation in the northern North Sea, whilst the variable stress orientations of the sedimentary sequence of the central North Sea are attributed to the decoupling of the stress regime from that of the basement by the Zechstein evaporites (Hillis & Nelson, 2005). Broadly, some areas of the British Isles and surrounding offshore basins exhibit plate-scale ~NW-SE $\sigma_{Hmax,}$ whereas in other areas σ_{Hmax} is controlled by major intraplate stress sources and more local-scale mechanical factors.

In this paper we present new borehole breakout data from 16 wells in the FSR based on four-arm caliper and dipmeter logs (Fig. 1). Maximum horizontal stress orientations from the majority of most wells are assigned a B or C-quality ranking, and hence are considered reliable. Though σ_{Hmax} orientations from wells located in the NE parts of the study area are broadly ~NW-SE, wells from the central and SW parts of the basin exhibit surprising variability, with a mixture of ~N-S, E-W and NE-SW σ_{Hmax} orientations. The latter trend is more common, and parallels the strikes of the main rift-bounding faults, which may have caused local perturbations to the stress pattern within the basin. When all the individual breakout orientations are aggregated, a dominant ~WNW-ESE σ_{Hmax} orientation emerges. This is similar to that observed in the adjacent East Shetland Basin, and is thus interpreted to represent the regional stress trend upon which local variations are superimposed. Our study also shows the need for a better understanding of the stress field in this region.

Geological Setting

Rifting along the Atlantic margin of NW Britain took place episodically from the Carboniferous until early Cenozoic (earliest Eocene) breakup. The Devono-Carboniferous basins are a relic of post-Caledonian orogenic collapse, whereas Permo-Triassic, (mainly Late) Jurassic, and Cretaceous basin development is related to the fragmentation of Pangaea, which ultimately led to continental breakup off NW Britain in Early Eocene time (Doré et al. 1999; Roberts et al. 1999). Throughout this protracted period of extension, the stress orientation rotated significantly, and resulted in the oblique overprinting of older rifts (i.e. Permian–Triassic and Jurassic rifts) by younger rifts (the Cretaceous–Cenozoic basins). This complex history of extension and rifting is well preserved in the FSR, where the sequential development of pre-, syn- and post-breakup basins is preserved as an asymmetrically-stacked (towards the ocean margin) series of structures (Fig. 3).

The structural framework illustrated in Fig. 1 is a legacy of the history of extension in the FSR, and for the most part reflects the syn-breakup (Paleocene–earliest Eocene) arrangement of highs and basins (Fig. 3). This framework was subsequently enhanced by post-breakup compressional tectonism, which accentuated structures, such as the Fugloy, Munkagrunnur and Wyville Thomson ridges, and helped to create the contemporary bathymetry of the West Shetland and Faroe shelves, separated by the Faroe-Shetland Channel (Stoker et al. 2010). Many of the structural highs within the Faroe–Shetland region comprise, or are underlain by, Archaean basement of Lewisian affinity (Ritchie et al. 2011a). The structural trend of the basement blocks is dominated by a NE-trending Caledonian structural grain, with this pattern also cut by NW-trending faults and transfer zones or lineaments (cf.

126 Ritchie et al. 2011b), though the existence and significance of these features is
127 debated (Moy & Imber, 2009).
128
129 **Methodology**
130 Borehole breakouts form when the concentrated stress around a wellbore
131 exceeds the compressive stress of the rock (Zoback et al., 1985). Conjugate shear
132 fractures in the side of the wellbore cause the rock to break off, resulting in the
133 wellbore being elongated in the direction perpendicular to σ_{Hmax} (Fig. 4a). These
134 elongated zones can be identified and measured using four-arm dipmeter or caliper
135 tools. Breakouts were carefully identified and distinguished from other borehole
136 elongations (e.g. washouts, key seats; Fig. 4b) using the criteria defined by Plumb &
137 Hickman (1985) and Reinecker et al. (2003). Breakouts can rotate in inclined
138 boreholes and do not always directly yield the horizontal stress orientation, though
139 boreholes with <20° deviaition in a normal or strike-slip faulting stress regime do not
140 show any significant rotation in orientation and still yield the approximate σ_{Hmax}
141 orientation (Peska & Zoback, 1995). Hence, breakouts were only used to estimate the
142 σ_{Hmax} orientation in wellbore intervals with deviations of <20°. The mean σ_{Hmax}
143 orientation from each well was given a quality ranking according to the most recent
144 World Stress Map (WSM) project criteria (Heidbach et al., 2010).
145
146 **Contemporary stress orientations**
147 Sixteen wells were analysed in this study. The majority (13) of these are
148 located in a ~200 km long zone within and immediately outside the main depocenter
149 of the structurally complex FSB, with individual wells targeting a variety of sub-
150 basins and structural highs (Fig. 1). Three additional wells are located >100 km to the

NE of this zone, and outside the limits of the FSB. All wells were drilled before 1993 and because resistivity image logs were not available, data from four-arm caliper and dipmeter tools were used to identify borehole breakouts from which σ_{Hmax} orientations have been determined (Fig. 4c). Image logs allow borehole breakouts (and drilling-induced tensile fractures) to be directly visualised and are now more prevalently used than four-arm caliper data, though with sufficient care the latter can be used to reliably determine breakout and thus stress orientations (Zoback, 2010).

A total of 202 breakouts with a combined length of ~3.2 km were interpreted in the 16 wells used in this study (Table 1). The breakouts covered a depth range from 662 to 5257 m. An example of breakouts identified in well 205/21-1A is provided in Fig. 4c. Four of the wells we analysed are assigned B-quality rankings for mean σ_{Hmax} orientations, eight are assigned C-quality rankings, and four are assigned D-quality rankings. The mean of the mean σ_{Hmax} orientations in all 16 wells is 086°N; the mean of the mean σ_{Hmax} orientations in all wells with B-C quality breakouts, which are considered to show the σ_{Hmax} orientations within ±25°, is 074°N. When all the individual unweighted breakouts from each well are aggregated, a dominant WNW-ESE σ_{Hmax} orientation is observed (Fig. 5), similar to that reported in the adjacent East Shetland Basin (Zanella & Coward, 2003). Following the approach of Hillis & Reynolds (2000, 2003) we applied a Rayleigh Test to the individual stress orientation data to investigate whether, and how strongly developed, any preferred stress orientation is within the study area. The Rayleigh Test determines the confidence level at which we can reject the null hypothesis that stress orientations within a given region are random (Mardia, 1972; Coblentz & Richardson, 1995). For the FSR, the null hypothesis can be rejected at a confidence level of at least 99.9%. However, it is

175 important to note that despite this result, there is considerable localised stress
176 variation within the FSR.

177 The three wells located in the NE of the study area (in the Møre and Magnus
178 basins and on the Erlend High, hereafter referred to as the NE province) reveal
179 broadly consistent, NW-SE to NNW-SSE σ_{Hmax} orientations (Fig. 1).

180 The wells located in the SW of the study area indicate more variable σ_{Hmax}
181 orientations (Fig. 1). This variability is most pronounced in the central FSR, which
182 includes the Foula and Flett sub-basins and the Rona and Flett Highs, hereafter
183 referred to as the central province. Eight wells are located in this area, with σ_{Hmax}
184 orientations that vary between 002 and 122°N. These eight wells demonstrate three
185 main trends; a N-S trend (including one B-quality indicator (214/27-1)), an E-W
186 trend, and a broadly NE-SW trend. The latter is defined by four wells, three of which
187 are assigned a D-quality ranking, but one well (206/05-1) has a B-quality ranking.

188 The four most southerly wells, which are located just outside the FSB and
189 hereafter referred to as the SW province, exhibit similar variability, with σ_{Hmax}
190 orientations that vary between 042 and 158°N (Fig. 1). Two of these wells have B-
191 quality rankings; 202/03a-3 where σ_{Hmax} is broadly ~NE-SW, and 205/21-1A where
192 σ_{Hmax} is E-W. Well 204/28-1 drilled on the Judd High, for which we determined a C-
193 quality σ_{Hmax} orientation of 158°N, is one of the wells for which a stress orientation
194 was determined by Klein & Barr (1986). These authors reported a C-quality ranked
195 σ_{Hmax} orientation of 145°N, in broad agreement with our analysis.

196

197 **Discussion**

198 A new analysis of borehole breakouts identified in 16 petroleum wells in the
199 FSR reveals unanticipated variability in σ_{Hmax} orientations. When all the unweighted

breakout data are aggregated, a dominant ~WNW-ESE σ_{Hmax} orientation is apparent, though within the study area, individual wells exhibit a mixture of ~N-S, NE-SW and NW-SE orientations, and three provinces with distinct sub-trends are identified (Fig. 5). This short-wavelength variation in σ_{Hmax} orientation contrasts with surrounding regions such as the British Isles where σ_{Hmax} orientations are dominantly ~NW-SE (Evans & Brereton, 1990; Baptie, 2010), though the ~WNW-ESE σ_{Hmax} orientation that emerges from the aggregated breakout data is similar to that observed in the adjacent East Shetland Basin (Zanella & Coward, 2003) (Fig. 2). Our results conflict with plate-scale modelling studies that predict consistently ~NW-SE σ_{Hmax} orientations throughout the FSR (Gölke & Coblentz, 1996). We note, however, that variable σ_{Hmax} orientations are observed in the central North Sea Basin (Hillis & Nelson, 2005) to the southeast of our study area. We interpret our results in terms of short-wavelength variations in σ_{Hmax} orientation that are superimposed upon a regional ~WNW-ESE trend that appears to be a continuation of that observed in the East Shetland Basin. In the following text we explore the likely sources of stress that are responsible for the variation in σ_{Hmax} orientation that we observe in the FSR

The increasing spatial density of stress information compiled by the WSM project in recent years has led to raised awareness of the forces that can cause stress field variations at more regional (100-500 km scales) and local (<100 km) spatial scales (Heidbach et al., 2007), appropriate to that of our study area. Regional-scale (second-order) stress fields are often profoundly influenced by lateral contrasts in lithospheric density and strength caused by rifting, isostatic compensation and topography, and by lithospheric flexure (e.g. due to deglaciation) (Heidbach et al., 2007). Local-scale (third-order) stress field variations from regional or plate-scale stress patterns may result from the presence of active or ‘weak’ faults, seismically

induced stress changes following earthquakes or volcanic eruptions, or from mechanical and density contrasts imparted by detachment layers or salt bodies (Heidbach et al., 2007; Tingay et al., 2012). In the following sections we examine which of these sources of crustal stresses may account for the observed variability in σ_{Hmax} orientations in the FSR.

Maximum horizontal stress orientations in many basins at passive, rifted continental margin settings similar to the FSR are typified by first-order stress fields (consistent over scales >500 km) controlled by plate boundary forces (Zoback, 1992; Hillis & Reynolds, 2000; Heidbach et al., 2010), with deviations from regional trends often due to gravitational potential stresses arising from variations in lithospheric structure between the passive margin and its (often significantly elevated) continental hinterland (Pascal & Cloetingh, 2009). Variable σ_{Hmax} orientations are observed in some continental margin basins where the sedimentary fill is undergoing gravity-driven collapse (Tingay et al., 2005; King et al., 2012). This most commonly occurs in active delta-deepwater fold-thrust belts, where gravitational potential of accumulating sediments on the delta top generates margin-parallel σ_{Hmax} orientations marked by normal growth faults, whilst compression in the delta toe is marked by imbricate thrusts and folding and margin-normal σ_{Hmax} orientations (King et al., 2012). A series of Paleocene–Plio-Pleistocene prograding clastic sedimentary wedges with a combined thickness of up to 4 km were deposited in the Faroe-Shetland Basin during the Cenozoic (Stoker et al., 2010; Stoker & Varming, 2011), but there is no evidence to suggest that this sequence is undergoing (or has experienced gravity-driven deformation in the recent geological past (Stoker & Varming, 2011)).

Loads that are imposed on, or that are within the lithosphere, can induce large flexural stresses that can perturb stress orientations over length scales of hundreds of

kilometres (Zoback, 2010). Grollimund et al. (2001) and Grollimund & Zoback (2003) have proposed that lithosphere flexure following the removal of the Fennoscandian ice sheet is a major source of lateral stress variations in the Norwegian sector of the northern North Sea, several hundred kilometres to the east of our study area. The three-dimensional modelling results of Grollimund & Zoback (2003) suggests that both the ~E-W σ_{Hmax} orientation observed in the northern North Sea, and the swing of σ_{Hmax} orientations from WNW-ESE in the East Shetland Basin, on the west side of the Viking Graben, to ENE-WSW on the east side of the graben can be explained by deglaciation-induced lithospheric flexure of the region adjacent to the ice sheet, superimposed on plate-driving stresses. Given that much of our study area lies close to the tentative limit of the confluent British and Fennoscandian ice sheets at the last glacial maximum (Bradwell et al., 2008; Stoker & Varming, 2011), it is possible that deglaciation-induced lithospheric flexure may have contributed to the observed σ_{Hmax} orientations in the FSR. We note that Pascal & Cloetingh (2009) have disputed the deglaciation hypothesis, claiming instead that the observed stress orientations in the northern North Sea reflect gravitational potential stresses arising from lithospheric structure. Irrespective of the causes, we suggest that the observed ~WNW-ESE σ_{Hmax} orientation that emerges when all individual breakouts are aggregated reflects a continuation of the broadly ~E-W σ_{Hmax} orientations that are observed in the East Shetland Basin and the northern North Sea (Fig. 2).

We argue that the short-wavelength (~10-50 km) variations in σ_{Hmax} orientations that are observed throughout the FSR, but which are particularly evident in the SW and central provinces within our study area, are probably caused by local sources of stress (i.e. within the basin itself) that superpose on the regional ~WNW-ESE σ_{Hmax} orientation. As mentioned earlier, local-scale (<100 km) variations in σ_{Hmax}

orientations may be influenced by pre-existing geological structures (e.g. faults, igneous intrusions), seismically induced stress changes following earthquakes or volcanic eruptions, or from mechanical and density contrasts imparted by detachment layers or salt bodies (Heidbach et al., 2007). Though there is abundant evidence for neotectonic fold growth in the FSR (the implications of which are explored in more detail later; Ritchie et al., 2008), there are very few recorded earthquakes within this study area that may have perturbed the stress field (Long et al., 2011).

Hillis & Nelson (2005) suggested that the variable σ_{Hmax} orientations of the central North Sea basin may be due to the extensive Zechstein halites, which may cause the stress regime in the overlying rocks of Triassic-Recent age to be detached from that of the basement, with far-field controlled, basement stresses not being transmitted above the Zechstein halites. Detached stress provinces have been described in many basins that contain evaporate sequences, with Tingay et al. (2012) providing a compelling recent example from the Nile Delta, where σ_{Hmax} orientations in sequences above and below the Messinian evaporates typically differ by ~60-90°. However, there are no known salt sequences within the FSR. Overpressured shales can also act as mechanical and structural detachments that may cause stress orientations to vary with depth in a basin (Heidbach et al., 2007). Thick shale sequences are found within the Campanian-Danian Sheltand Group (Stoker & Ziska, 2011), and a previous study by the authors has demonstrated that these shales are often overpressured at depths >3 km (Tassone et al., 2014). We note that individual wells in our study area do not provide evidence for any systematic variation in breakout orientation with depth, and thus we think it unlikely that the observed variation in σ_{Hmax} orientation is caused by mechanically weak shale sequences.

Many authors have described local stress variations, of the order of a few metres to several kilometres, near geological structures such as faults, fractures or igneous intrusions (e.g. Bell, 1996; Yale, 2003; Morley, 2010; Tingay et al., 2010; Fig. 6). Such variations are commonly considered to result from geological structures acting as mechanical discontinuities. Principal stresses intersect free surfaces at right angles, so if a geological structure acts as a free surface it will deflect a principal stress unless that stress happens to be oriented exactly perpendicular to the surface, with the nature of the interface and the geomechanical property contrast determining the scale over which horizontal principal stresses are deflected (Bell, 1996). In general, it is predicted that σ_{Hmax} will be deflected sub-parallel to mechanically weak structures such as open fractures or weak fault zones, and deflected perpendicular to mechanically stiff or hard structures such as cemented fault zones or igneous intrusions (Bell, 1996) (Fig. 6a, b).

The FSR was the site of substantial magmatic activity during the Early Paleocene and latest Paleocene to Early Eocene, and hence the Eocene and older sedimentary sequences in this region contain a large number of lava fields, volcaniciclastic units and intrusive complexes (Passey & Hitchen, 2011; Schofield et al., 2012, in review). If these igneous rocks act as harder or stiffer zones relative to the surrounding sedimentary rocks, they could potentially cause deflections of σ_{Hmax} orientations. The densest concentration of igneous rocks in the study area occurs in the central FSB (Rateau et al., 2013; Schofield et al., in review), where σ_{Hmax} orientations are highly variable. Within this area, we have identified breakouts in four wells which also penetrated intrusions (205/10-2B, 214/27-1, 214/28-1 and 219/20-1); several of the other wells in this area are located in close proximity to intrusions. However, we note that σ_{Hmax} orientations determined for wells in the SW province,

where few volcanic and intrusive sequences have been identified within the subsurface, are also highly variable (Fig. 1). Furthermore, well 209/03-1A, which is located in the NE province, penetrated >800 m of Early Eocene basaltic lavas that form part of the Erlend Volcanic Centre (Passey & Hitchen, 2011). We identified numerous breakouts within this basaltic sequence, from which we determined a B-quality σ_{Hmax} orientation of 126°N. This orientation is consistent with those determined for other wells in the NE of the FSR, which indicate a ~NE-SW σ_{Hmax} orientation (Fig. 1). Thus whilst we cannot rule out a contribution from stress perturbations around igneous bodies to the variation in σ_{Hmax} orientation in the central province, our observations from the SW and NE provinces are not consistent with igneous bodies exerting a first-order control on stress orientations.

We suggest that the localized stress perturbations that are particularly evident in the SW and central provinces within our study area, are most likely a consequence of the complicated framework of fault-bounded structural highs in these regions (Ritchie et al., 2011b) (Fig. 3b). This framework was established syn-breakup (Paleocene–earliest Eocene), and subsequently enhanced by post-breakup compressional tectonism (Stoker et al., 2010). A large number of wells located in close proximity to fault-bounded structural highs exhibit σ_{Hmax} orientations that are either parallel or sub-parallel to the strikes of the bounding faults. In the SW province, wells 202/03a-3 and 204/28-1 are located ~20 km apart but exhibit markedly different σ_{Hmax} orientations. Well 202/03-a3 is located in the West Solan Basin and exhibits a ~ENE-WSW σ_{Hmax} orientation, sub-parallel to a major ENE-WSW-striking normal fault that bounds the southeastern side of the Judd High. Well 204/28-1, which exhibits a NNW-SSE σ_{Hmax} orientation, was drilled on the Judd High in the footwall of the Judd Fault, which in the vicinity of this well strikes ~NW-SE (Fig. 1). Well

205/21-1a, which exhibits a B-quality, ~E-W σ_{Hmax} orientation sub-parallel to the strike of a nearby fault that causes significant offset within the Upper Cretaceous sequence, which is shown in Fig 3b. Caliper log data from this well with interpreted breakouts within the Upper Cretaceous section is presented in Fig. 4c.

In the central province, three wells located in the Foula sub-basin (206/3-1, 206/5-1, 214/29-1) exhibit ENE-WSW to NE-SW σ_{Hmax} orientations, including one B-quality measurement (206/5-1). These three wells are proximal to the Rona Fault, a major normal fault that juxtaposes the basin fill against crystalline basement and which trends broadly NE-SW (i.e. parallel/sub-parallel to the determined σ_{Hmax} orientations). Other wells in this part of the study are where σ_{Hmax} orientations appear to be parallel or sub-parallel to normal faults that structural highs include 205/20-1, 205/10-2B and 214/27-1 (Fig. 1).

A notable exception is provided by well 206/8-5, which exhibits a WNW-ESE σ_{Hmax} orientation. This well targeted the core of the Clair Field, a sequence of oil-bearing Carboniferous-Devonian clastic rocks situated beneath Upper Cretaceous mudstones and above fractured Lewisian basement (Coney et al., 1993). The Clair Field, the outline of which is shown in Figure 1, is located on the Rona High, an elongate basement ridge cored by crystalline Lewisian rocks (Quinn et al., 2011). The Rona High trends NE-SW, and the Clair Field is offset by a series of ~NE-SW trending faults (Olgivie et al., 2015). In this case therefore, the σ_{Hmax} orientation is near-perpendicular to the local structural trend.

We note that the Clair Field is one of few areas within the FSR for which independent constraints on the orientation of σ_{Hmax} are available. Smith & McGarrity (2001) reported a σ_{Hmax} orientation of 104°N ± 18° for well 206/8-9y based on a 'borehole stress analysis'. Though these authors did not describe the types of data or

observations used to constrain the orientation of σ_{Hmax}, they also reported that the strikes of the majority of open fractures (which are presumably critically stressed) recorded in the well were ~110-120°N, implying these fractures are critically stressed. The principal orientation of open fractures in the nearby well 206/8-8 is very similar (~105°N), with a secondary NNW-SSE trend also reported (Coney et al., 1993). Previous data from the Clair Field thus support our results, which indicate a WNW-ESE σ_{Hmax} orientation.

The observation that σ_{Hmax} orientations in the SW and central provinces are typically parallel or sub-parallel to the margins of the intra-basin structural highs near which they were drilled implies that the normal faults that bound these highs may be weak relative to their surrounding rocks, causing stresses to be deflected such that the orientation of σ_{Hmax} parallels the faults (Fig. 6). Reorientations of σ_{Hmax} associated with nearby faults are observed in many basins covering a range of tectonic environments (Bell, 1996; Reynolds & Hillis, 2000; Townend & Zoback, 2004; Tingay et al., 2010). Though the simple model presented in Figure 6b accounts for stress deflections due to weak faults in plan view only, the observation that faults with a variety of geometric attributes and structural histories are associated with stress deflections suggests that the model can be extended to explain stress deflections in three-dimensions (Fig. 6c). Yale (2003) provides several convincing examples of stress deflections at distances of up to several kilometres from faults in the southern and northern North Sea basins, and has suggested that the smaller the difference between the magnitudes of the minimum and maximum horizontal stresses, the larger the influence of the fault is. We have not constrained the full stress tensor in this study, and more critically, we are not aware of any datasets that constrain the relative and absolute strength (or weakness) of fault rocks in the FSR, and until such datasets

399 are available, or indeed more σ_{Hmax} measurements exist, our suggestion that weak
400 faults have caused stress reorientations must remain speculative. However, this notion
401 has some support from studies of fault reactivation in regions adjacent to the FSR.
402 It is generally agreed that the reactivation of basement fabrics has played a
403 major role in determining the structural architecture of the rift basins of the NE
404 Atlantic margin, where the dominant structural trends (N-S to NE-SW and ESE-
405 WNW to SE-NW) are strikingly similar to regional structural trends in exposures of
406 Palaeozoic and Proterozoic basement rocks onshore (Doré et al., 1997; Wilson et al.,
407 2010). In the FSR, the development of normal faults from the Permian onwards has
408 been strongly influenced by pre-existing, NE-SW trending Caledonian structures
409 (Ritchie et al., 2011). The Outer Hebrides Fault Zone (OHFZ), which crops out for
410 ~190 km along the east coast of the Outer Hebrides, to the SW of our study area,
411 provides a useful case study of the repeated reactivation of basement fabrics. The
412 OHFZ is a crustal-scale ESE-dipping fault zone between 1 and 6 km thick that cross-
413 cuts preexisting, high-grade gneisses of the Archaean to Palaeoproterozoic Lewisian
414 Complex (Imber et al., 1997). The OHFZ records a complicated kinematic history
415 with repeated phases of reactivation, which culminated in its extensional dip-slip
416 reactivation during the Mesozoic, resulting in the formation of the ~NE-SW trending
417 Minch Fault that bounds the Minch and Sea of Hebrides rift basins (Roberts &
418 Holdsworth, 1999). Detailed microstructural studies of fault rock assemblages by
419 Imber et al. (1997, 2001) suggest that the long-lived displacement history of the
420 OHFZ is largely due to the widespread presence of weak (in an absolute sense), fine-
421 grained phyllosilicate-bearing fault rocks (phyllonites).
422

Circumstantial evidence for the existence of weak faults in the FSR is provided from the Victory gas discovery (location shown in Figure 1). Victory is situated toward the north-eastern end of the Rona High, with the hydrocarbons trapped in Lower Cretaceous sandstones in a south-easterly dipping tilted fault block that is bounded by a NE-trending fault (Quinn et al., 2011). The structure contains residual biodegraded oil within and below the current gas column, which occupies less than half of the vertical closure of the structure (Doré et al., 2002). Repeated reactivation of this NE-trending, presumably weak fault throughout the late Cretaceous-Palaeogene is thought to have caused the breach and leakage of the early oil charges (Goodchild et al., 1999). Based on sonic velocity analysis of overcompacted Upper Cretaceous marine shales in the FSR, Tassone et al. (2014) identified several hundred metres of exhumation along the northeastern Rona High, which most likely took place during the Oligocene to mid-Miocene and was related to the reactivation of the faults that bound the structural high.

Stress reorientations within or close to faults have also been ascribed to changes in the bulk elastic properties that occur within the highly-fractured damage zones that surround the fault core, which typically encompass distances in the order of 10's to 100's of m (Faulkner et al., 2006, 2011; Morley, 2010). Most of the wells in our study area are located at distances of up to several km from the most proximal basement-involved faults and hence most probably outside their damage zones. However, the distances perpendicular to faults over which stress rotations are observed in the FSR are consistent with those observed in other regions such as the southern and northern North Sea basins (Yale, 2003).

We note that, though few in number, our stress measurements from the NE province indicate a ~NW-SE σ_{Hmax} orientation which is broadly consistent with existing measurements from the adjoining East Shetland Basin (Zanella & Coward, 2003), and with the P-axis orientation (107°N) of a magnitude 4.7 reverse-fault regime earthquake that occurred in the northeast of the basin in 2007 at a depth of ~12 km; this event is included in the 2008 WSM release and is assigned a C-quality ranking. These ~NW-SE σ_{Hmax} orientations are orthogonal to the axes of a series of NE- and NNE-trending Cenozoic-age growth folds described by Ritchie et al. (2003, 2008), which are inferred to have grown under a compressional stress regime, some of which were active as recently as the early Pliocene. We speculate that in the NE of the FSR, where the Cretaceous-Cenozoic sedimentary succession is thicker and the underlying structural configuration is somewhat less complicated (Ritchie et al., 2011a) in comparison to the central and SW provinces (Fig. 3), stress perturbations around faults is less prominent and thus σ_{Hmax} orientations reflect the regional ~NW-SE trend across much of NW Europe that is primarily controlled by plate boundary forces (Fig. 6c).

We close by emphasizing several important uncertainties associated with our results. We have analyzed only a small number of wells in the FSR, and our σ_{Hmax} orientations have been determined using breakouts identified on caliper logs rather than resistivity and acoustic image logs that allow direct visualization and thus interpretation of breakouts. Because our results contain a number of B and C-quality ranked σ_{Hmax} orientations, we are confident that the observed variation in σ_{Hmax} in the FSR is a real phenomenon. Furthermore, the few published σ_{Hmax} orientations in this region are generally consistent with those we have determined for the same, or nearby wells. However, substantially more results from a variety of reliable stress indicators

472 are needed in order to achieve a better understanding of the stress field along this
473 critical part of the NE Atlantic continental margin.
474
475 **Conclusions**
476 The Faroe-Shetland Region of the NE Atlantic continental margin contains a
477 number of Mesozoic-Palaeogene-age rift basins that have experienced a multi-phase
478 rifting history that resulted in a complex arrangement of intra-basinal structural highs,
479 followed by a complicated post-breakup history characterized by magmatism,
480 compressional tectonics and uplift. There is strong interest in better understanding
481 both the Cenozoic tectonic evolution of this basin and its potential hydrocarbon
482 resources. It is thus somewhat surprising that there are very few published
483 contemporary stress measurements in this region (where >160 petroleum wells have
484 been drilled) in comparison to surrounding areas such as the British Isles and North
485 Sea Basin. The orientation of the maximum horizontal compressional stress (σ_{Hmax})
486 across most of NW Europe is ~NW-SE, which is generally agreed to reflect a first-
487 order control by plate boundary forces. Modeling studies predict similarly oriented
488 ~NW-SE σ_{Hmax} throughout the FSR, though deviations from this trend in adjacent
489 parts of the North Sea Basin are observed and have been attributed to second and
490 third-order sources of stress such as flexural rebound following deglaciation and
491 mechanical contrasts caused by geological structures. We have determined 16 B-D
492 quality (12 B-C) σ_{Hmax} orientations based on borehole breakouts interpreted from
493 caliper logs acquired in petroleum wells in the FSR. When all the individual
494 breakouts are aggregated, a broadly ~WNW-ESE σ_{Hmax} orientation is indicated for the
495 FSR, consistent with that reported for adjacent East Shetland Basin. Contemporary
496 stress orientations in the NE of the study area are ~NW-SE, consistent with the

regional pattern of stresses in NW Europe, and with the strikes of compressional growth folds that have been active as recent as the Pliocene. However, contemporary stress orientations in the central and SW of the study area exhibit considerable short-wavelength (distances <10-50 km) variation, with NE-SW, N-S and E-W orientations. These are inconsistent with the regional pattern of stresses in NW Europe, but are parallel or sub-parallel to underlying structural trends, and suggest the superposition of local-scale causes of stress. We interpret this complex pattern of stress orientations in terms of stress deflections towards weak faults that downthrow the Mesozoic-Cenozoic sedimentary successions of the FSR against structural highs cored by Proterozoic-Achaean basement rocks. This notion has some support from fault studies in onshore exhumed basin regions, which have shown that similar faults to those that likely bound structural highs offshore are characterized by mechanically weak fault rock assemblages. However, substantially more results from a variety of reliable stress indicators are needed in order to achieve a better understanding of the stress field along this critical part of the NE Atlantic continental margin.

Acknowledgments and Funding

This work was funded by ARC Discovery Project DP0879612, ASEG Research Foundation Project RF09P04 and represents TRaX contribution 325. We thank Sandy Henderson for his assistance with data loading, and gratefully acknowledge the British Geological Survey for access to well-log data and hospitality during visits by SPH and DRT. We also thank Jonny Imber for a constructive review. The contribution of Stoker is made with the permission of the Director of the British Geological Survey (Natural Environmental Research Council).

References

Austin, J.A., Cannon, S.J.C. & Ellis, D. 2014. Hydrocarbon exploration and exploitation West of Shetlands. *In:* Cannon, S.J.C. & Ellis, D. (eds) *Hydrocarbon exploration to exploitation West of Shetlands.* Geological Society, London, Special Publications, **397,** 1-10.

Baptie, B. 2010. Seismogenesis and state of stress in the UK. *Tectonophysics,* **482,** 150-159.

Bell, J.S. 1996. In situ stresses in sedimentary rocks (part 2): applications of stress measurements. *Geoscience Canada,* **23,** 135-153.

Bradwell, T., Stoker, M.S., Golledge, N., Wilson, C., Merritt, J., Long, D., Everest, J., Hestvik, O.B., Stevenson, A.G., Hubbard, A., Finlayson, A. & Mathers, H. 2008. The northern sector of the last British Ice Sheet: maximum extent and demise. *Earth Science Reviews,* **88,** 207-226.

Coblentz, D. & Richardson, R.M. 1995. Statistical trends in the intraplate stress field. *Journal of Geophysical Research,* **100,** 20245-20255.

Coney, D., Fyfe, T.B., Retail, P. & Smith, P.J. 1993. Clair appraisal: the benefits of a co-operative approach. *In:* Parker, J.R. (ed.) *Petroleum Geology of Northwest Europe: Proceedings of the 4th Conference* (Ed. by J.R. Parker), Geological Society, London, 1409-1420.

DECC Promote. 2014. Prospectivity in the UKCS north of 62°N. *Department of Energy & Climate Change, Promote United Kingdom 2014.*

Doré, A.G., Lundin, E.R., Fichler, C. & Olesen, O. 1997. Patterns of basement structure and reactivation along the NE Atlantic margin. *Journal of the Geological Society,* **154,** 85-92.

546 Doré, A.G., Lundin, E.R., Jensen, L.N., Birkeland, Ø., Eliassen, P.E. & Filcher, C.
547 1999. Principal tectonic events in the evolution of the northwest European
548 Atlantic margin. *In*: Fleet, A.J. & Boldy, S.A.R. (eds) *Petroleum Geology of*
549 *Northwest Europe: Proceedings of the 5th Conference,* Geological Society,
550 London, 41-61.
551 Doré, A.G., Corcoran, D.V. & Scotchman, I.C. 2002. Prediction of the hydrocarbon
552 system in exhumed basins, and application to the NW European margin. *In:*
553 Doré, A.G., Cartwright, J.A., Stoker, M.S., Turner, J.P. & White, N. (eds)
554 *Exhumation of the North Atlantic Margin: Timing, Mechanisms and*
555 *Implications for Petroleum Exploration.* Geological Society, London, Special
556 Publications, **196,** 401-429.
557 Ellis, D. & Stoker, M.S. 2014. The Faroe–Shetland Basin: a regional perspective from
558 the Paleocene to the present day and its relationship to the opening of the North
559 Atlantic Ocean. *In:* Cannon, S.J.C. & Ellis, D. (eds) *Hydrocarbon exploration*
560 *to exploitation West of Shetlands.* Geological Society, London, Special
561 Publications, **397,** 11-31.
562 Evans, C.J. & Brereton, N.R. 1990. In situ crustal stress in the United Kingdom from
563 borehole breakouts. *In:* Hurst, A., Lovell, M.A. & Morton, A.C. (eds)
564 *Geological Applications of Wireline Logs.* Geological Society, London, Special
565 Publications, **48,** 327-338.
566 Faulkner, D.R., Mitchell, T.M., Healy, D. & Heap, M.J. 2006. Slip on 'weak' faults
567 by the rotation of regional stress in the fracture damage zone. *Nature,* **444,** 922-
568 925.
569 Faulkner, D.R., Mitchell, T.M., Jensen, E. & Cembrano, J. 2011. Scaling of fault
570 damage zones with displacement and the implications for fault growth

processes. *Journal of Geophysical Research,* **116,** B05403, doi:10.1029/2010JB007788.

Gölke, M. & Coblentz, D. 1996. Origins of the European regional stress field. *Tectonophysics,* **266**, 11-24.

Goodchild, M.W., Henry, K.L., Hinkley, R.J. & Imbus, S.W. 1999. The Victory gas field, West of Shetland. *In*: Fleet, A.J. & Boldy, S.A.R. (eds) *Petroleum Geology of Northwest Europe: Proceedings of the 5th Conference,* Geological Society, London, 713-724.

Grollimund, B., Zoback, M.D., Wiprut, D.J. & Arnesen, L. 2001. Stress orientation, pore pressure and least principal stress in the Norwegian sector of the North Sea. *Petroleum Geoscience,* **7,** 173-180.

Grollimund, B. & Zoback, M.D. 2003. Impact of glacially induced stress changes on fault-seal integrity offshore Norway. *AAPG Bulletin,* **87,** 493-506.

Hartley, R.A., Roberts, G.G., White, N. & Richardson, C. 2011. Transient convective uplift of an ancient buried landscape. *Nature Geoscience,* **4**, 562-565.

Heidbach, O., Reinecker, J., Tingay, M., Müller, B., Sperner, B., Fuchs, K. & Wenzel, F. 2007. Plate boundary forces are not enough: second- and third-order stress patterns highlighted in the World Stress Map database. *Tectonics,* **26,** TC6014. doi:10.1029/2007TC002133.

Heidbach, O., Tingay, M., Barth, A., Reinecker, J., Kurfeß, D. & Müller, B. 2008. The World Stress Map database release 2008. doi:10.1594/GFZ.WSM.Rel2008

Heidbach, O., Tingay, M., Barth, A., Reinecker, J., Kurfeß, D. & Müller, B. 2010. Global crustal stress pattern based on the World Stress Map database release 2008. *Tectonophysics,* **482,** 3-15.

Hillis, R.R. & Nelson, E.J. 2005. *In situ* stresses in the North Sea and their

applications: petroleum geomechanics from exploration to development. *In:* Doré, A.G. & Vining, B.A. (eds) *Petroleum Geology: North-West Europe and Global Perspectives – Proceedings of the 6th Petroleum Geology Conference.* Geological Society, London, 551-564.

Hillis, R.R. & Reynolds, S.D. 2000. The Australian stress map. *Journal of the Geological Society,* **157,** 915-921.

Hillis, R.R. & Reynolds, S.D. 2003. In situ stress field of Australia. *In:* Hillis, R.R. & Müller, R.D. (eds) *Evolution and Dynamics of the Australian Plate.* Geological Society of Australia, Special Publication **22,** 49-58.

Hillis, R.R., Holford, S.P., Green, P.F., Doré, A.G., Gatliff, R.W., Stoker, M.S., Thomson, K., Turner, J.P., Underhill, J.R. & Williams, G.A. 2008. Cenozoic exhumation of the southern British Isles. *Geology,* **36,** 371-374.

Holford, S.P., Green, P.F., Turner, J.P., Williams, G.A., Hillis, R.R., Tappin, D.R. & Duddy, I.R. 2008. Evidence for km-scale Neogene exhumation driven by compressional deformation in the Irish sea basin system. *In:* Johnson, H., Doré, A.G., Gatliff, R.W., Holdsworth, R., Lundin, E. & Ritchie, J.D. (eds) *The Nature and Origin of Compression in Passive Margins.* Geological Society, London, Special Publications, **306,** 91-119.

Holford, S.P., Green, P.F., Duddy, I.R., Turner, J.P., Hillis, R.R. & Stoker, M.S. 2009. Regional intraplate exhumation episodes related to plate boundary deformation. *GSA Bulletin,* **121,** 1611-1628.

Holford, S.P., Green, P.F., Hillis, R.R., Underhill, J.R., Stoker, M.S. & Duddy, I.R. 2010. Multiple post-Caledonian exhumation episodes across NW Scotland revealed by apatite fission-track analysis. *Journal of the Geological Society,* **167,** 675–694.

621 Imber, J., Holdsworth, R.E., Butler, C.A. & Lloyd, G.E. 1997. Fault-zone weakening
622 processes along the reactivated Outer Hebrides Fault Zone, Scotland. *Journal of*
623 *the Geological Society,* **154,** 105–109.
624 Imber, J., Holdsworth, R.E., Butler, C.A. & Strachan, R.A. 2001. A reappraisal of the
625 Sibson–Scholz fault zone model: The nature of the frictional to viscous
626 ("brittle-ductile") transition along a long-lived, crustal-scale fault, Outer
627 Hebrides, Scotland. *Tectonics,* **20,** 601–624.
628 King, R., Backé, G., Tingay, M., Hillis, R. & Mildren, S. 2012. Stress deflections
629 around salt diapirs in the Gulf of Mexico. *In:* Healy, D., Butler, R.W.H.,
630 Shipton, Z.K. & Sibson, R.H. (eds) *Faulting, Fracturing and Igneous Intrusion*
631 *in the Earth's Crust.* Geological Society, London, Special Publications, **367,**
632 141-153.
633 Klein, R.J. & Barr, M.V. 1986. Regional state of stress in Western Europe. *In:*
634 *Proceedings of the International Symposium on Rock Stresses and Rock Stress*
635 *Measurement.* Lulea, CENTEK, 33-44.
636 Lamers, E. & Carmichael, S.M.M. 1999. The Paleocene deep-water sandstone play
637 West of Shetland. *In*: Fleet, A.J. & Boldy, S.A.R. (eds) *Petroleum Geology of*
638 *Northwest Europe: Proceedings of the 5th Conference,* Geological Society,
639 London, 645-659.
640 Long, D., Ziska, H. & Musson, R. 2011. Geohazards. *In:* Ritchie, J.D., Ziska, H.,
641 Johnson, H. & Evans, D. (eds) *Geology of the Faroe-Shetland Basin and*
642 *adjacent areas.* British Geological Survey and Jarõfeingi Research Report
643 RR/11/01, 239-253.
644 Mardia, K.V. 1972. *Statistics of Directional Data.* Academic Press, New York.

Müller, B., Zoback, M.L., Fuchs, K., Mastin, L., Gregersen, S., Pavoni, N., Stephansson, O. & Ljunggren, C. 1992. Regional patterns of tectonic stress in Europe. *Journal of Geophysical Research,* **97,** 11783-11803.

Morley, C.K. 2010. Stress re-orientation along zones of weak fabrics in rifts: An explanation for pure extension in 'oblique' rift segments? *Earth and Planetary Science Letters,* **297,** 667-673.

Moy, D.J. & Imber, J. 2009. A critical analysis of the structure and tectonic significance of rift-oblique lineaments ('transfer zones') in the Mesozoic–Cenozoic succession of the Faroe–Shetland Basin, NE Atlantic margin. *Journal of the Geological Society*, **166**, 831–844.

Narayanasamy, R., Barr, D. & Milne, A. 2010. Wellbore-instability predictions within the Cretaceous mudstones, Clair Field, West of Shetlands. *SPE Drilling & Completion,* 518-529.

Olgivie, S., Barr, D., Roylance, P. & Dorling, M. 2015. Structural geology and well planning in the Clair Field. *In:* Richards, F.L., Richardson, N.J., Rippington, S.J., Wilson, R.W. & Bond, C.E. (eds) *Industrial Structural Geology: Principles, Techniques and Integration.* Geological Society, London, Special Publications, **321,** http://dx.doi.org/10/1144/SP421.7

Pascal, C. & Cloetingh, S.A.P.L. 2009. Gravitational potential stresses and stress field of passive continental margins: Insights from the south-Norway shelf. *Earth & Planetary Science Letters,* **277,** 464-473.

Passey, S. & Hitchen, K. 2011. Cenozoic (igneous). *In:* Ritchie, J.D., Ziska, H., Johnson, H. & Evans, D. (eds) *Geology of the Faroe-Shetland Basin and adjacent areas.* British Geological Survey and Jarõfeingi Research Report RR/11/01, 209-228.

Peška, P. & Zoback, M.D. 1995. Compressive and tensile failure of inclined well bores and determination of in situ stress and rock strength. *Journal of Geophysical Research,* **100,** 12791-12811.

Plumb, R.A. & Hickman, S.H. 1985. Stress-induced borehole elongation: A comparison between the four-arm dipmeter and the borehole televiewer in the Auburn Geothermal Well. *Journal of Geophysical Research,* **90,** 5513-5521.

Quinn, M., Varming, T. & Ólavsdottir, J. 2011. Petroleum geology. *In:* Ritchie, J.D., Ziska, H., Johnson, H. & Evans, D. (eds) *Geology of the Faroe-Shetland Basin and adjacent areas.* British Geological Survey and Jarõfeingi Research Report RR/11/01, 254-280.

Reinecker, J., Tingay, M. & Müller, B. 2003. Borehole breakout analysis from four-arm caliper logs. *World Stress Map Project Stress Analysis Guidelines,* http://www.world-stress-map.org

Reynolds, S.D. & Hillis, R.R. 2000. The in situ stress field of the Perth Basin, Australia. *Geophysical Research Letters,* **27,** 3421-3424.

Ritchie, J.D., Johnson, H. & Kimbell, G.S. 2003. The nature and age of Cenozoic contractional deformation within the Faroe-Shetland Basin. *Marine and Petroleum Geology,* **20,** 399-409.

Ritchie, J.D., Johnson, H., Quinn, M.F. & Gatliff, R.W. 2008. The effects of Cenozoic compression within the Faroe-Shetland Basin and adjacent areas. *In:* Johnson, H., Doré, A.G., Gatliff, R.W., Holdsworth, R., Lundin, E. & Ritchie, J.D. (eds) *The Nature and Origin of Compression in Passive Margins.* Geological Society, London, Special Publications, **306,** 121-136.

Ritchie, J.D., Ziska, H., Kimbell, G., Quinn, M. & Chadwick, A. 2011a. Structure. *In:* Ritchie, J.D., Ziska, H., Johnson, H. & Evans, D. (eds) *Geology of the Faroe-*

Shetland Basin and adjacent areas. British Geological Survey and Jarõfeingi Research Report RR/11/01, 9-70.

Ritchie, J.D., Noble, S., Darbyshire, F., Millar, I. & Chambers, L. 2011b. Pre-Devonian. *In:* Ritchie, J.D., Ziska, H., Johnson, H. & Evans, D. (eds) *Geology of the Faroe-Shetland Basin and adjacent areas.* British Geological Survey and Jarõfeingi Research Report RR/11/01, 71-78.

Roberts, A.M. & Holdsworth, R.E. 1999. Linking onshore and offshore structures: Mesozoic extension in the Scottish Highlands. *Journal of the Geological Society,* **156,** 1061-1064.

Roberts, D.G., Thompson, M., Mitchener, B., Hossack, J., Carmichael, S. & Bjørnseth, H.M. 1999. Palaeozoic to Tertiary rift and basin dynamics: mid-Norway to the Bay of Biscay – a new context for hydrocarbon prospectivity in the deep water frontier. *In*: Fleet, A.J. & Boldy, S.A.R. (eds) *Petroleum Geology of Northwest Europe: Proceedings of the 5th Conference,* Geological Society, London, 7-40.

Schofield, N., Heaton, L., Holford, S.P., Archer, S.G., Jackson, C.A.-L. & Jolley, D.W. 2012. Seismic imaging of 'broken bridges': linking seismic to outcrop-scale investigations of intrusive magma lobes. *Journal of the Geological Society,* **169,** 421-426.

Schofield, N. & Jolley, D.W. 2013. Development of intra-basaltic lava field drainage systems within the Faroe-Shetland Basin. *Petroleum Geoscience,* **19,** 259-272.

Schofield, N., Holford, S., Millet, J., Brown, D., Jolley, D., Passey, S., Muirhead, D., Grove, C., Magee, C., Murray, J., Hole, M., Jackson, C. & Stevenson, C. In review. Regional magma plumbing and emplacement mechanisms of the Faroe-

719 Shetland Sill Complex (FSSC): Implications for our understanding of magma
720 movement within sedimentary basins. *Basin Research.*
721 Smith, R.L. & McGarrity, J.P. 2001. Cracking the fractures – seismic anisotropy in an
722 offshore reservoir. *The Leading Edge,* **20,** 18-26.
723 Stoker, M.S. & Varming, T. 2011. Cenozoic (sedimentary). *In:* Ritchie, J.D., Ziska,
724 H., Johnson, H. & Evans, D. (eds) *Geology of the Faroe-Shetland Basin and*
725 *adjacent areas.* British Geological Survey and Jarõfeingi Research Report
726 RR/11/01, 151-208.
727 Stoker, M.S., Hoult, R.J., Nielsen, T., Hjlestuen, B.O., Laberg, J.S., Shannon, P.M.,
728 Praeg, D., Mathiesen, A., Van Weering, T.C.E. & McDonnell, A. 2005.
729 Sedimentary and oceanographic responses to early Neogene compression on the
730 NW European margin. *Marine and Petroleum Geology,* **22,** 1031–1044.
731 Stoker, M.S., Holford, S.P., Hillis, R.R., Green, P.F. & Duddy, I.R. 2010. Cenozoic
732 post-rift sedimentation off northwest Britain: recording the detritus of episodic
733 uplift on a passive continental margin. *Geology,* **38,** 595–598.
734 Tassone, D.R., Holford, S.P., Stoker, M.S., Green, P.F., Johnson, H., Underhill, J.R.
735 & Hillis, R.R. 2014. Constraining Cenozoic exhumation in the Faroe-Shetland
736 region using sonic transit time data. *Basin Research,* **26,** 38-72.
737 Tingay, M.R.P., Hillis, R.R., Morley, C.K., Swarbrick, R.E. & Drake, S.J. 2005.
738 Present day stress orientation in Brunei: a snapshot of 'prograding tectonics' in
739 a Tertiary delta. *Journal of the Geological Society,* **162,** 39-49.
740 Tingay, M.R.P., Morley, C., Hillis, R.R. & Meyer, J.J. 2010. Present-day stress
741 orientation in Thailand's basins. *Journal of Structural Geology,* **32,** 235-248.
742 Tingay, M., Bentham, P., De Feyter, A. & Kellner, A. 2012. Evidence for non-
743 Andersonian faulting above evaporites in the Nile Delta. *In:* Healy, D., Butler,

R.W.H., Shipton, Z.K. & Sibson, R.H. (eds) *Faulting, Fracturing and Igneous Intrusion in the Earth's Crust.* Geological Society, London, Special Publications, **367,** 155-170.

Townend, J. & Zoback, M.D. 2004. Regional tectonic stress near the San Andreas fault in central and southern California. *Geophysical Research Letters,* **31**, L15S11, doi:10.1029/2003GL018918.

Wilson, R.W., Holdsworth, R.E., Wild, L.E., McCaffrey, K.J.W., England, R.W., Imber, J. & Strachan, R.A. 2010. Basement-influenced rifting and basin development: a reappraisal of post-Caledonian faulting patterns from the North Coast Transfer Zone, Scotland. *In:* Law, R.D., Butler, R.W.H., Holdsworth, R.E., Krabbendam, M. & Strachan, R.A. (eds) *Continental Tectonics and Mountain Building: The Legacy of Peach and Horne.* Geological Society, London, Special Publications, **335,** 795-826.

Yale, D.P. 2003. Fault and stress magnitude controls on variations in the orientation of in situ stress. *In:* Ameen, S.A. (ed.) Fracture and In-Situ Stress Characterization of Hydrocarbon Reservoirs. Geological Society, London, Special Publications, **209,** 55-64.

Zanella, E. & Coward, M.P. 2003. Structural framework. *In:* Evans, D., Graham, C., Armour, A. & Bathurst, P. (eds) *The Millennium Atlas: Petroleum Geology of the Central and Northern North Sea.* Geological Society, London, 45-59.

Zoback, M.D., Moos, D., Mastin, L. & Anderson, R.N. 1985. Well bore breakouts and in situ stress. *Journal of Geophysical Research,* **90,** 5523-5530.

Zoback, M.L. 1992. First- and second-order patterns of stress in the lithosphere: the World Stress Map Project. *Journal of Geophysical Research,* **97,** 11703-11728.

Zoback, M.D. 2010. *Reservoir Geomechanics.* Cambridge University Press.

Figure captions

Figure 1

Contemporary stress orientations in the Faroe Shetland Region. Orientations determined in this study are denoted by white fills, with previous stress measurements denoted by grey fills. Wells 1-4 comprise the SW stress province, 5-13 the central stress province, and 14-16 the NE stress province. Structural elements are based on Ritchie et al. (2011a), to which the reader is referred for more detailed information.

Figure 2

Map showing published contemporary stress orientations from the British Isles, North Sea, western Scandinavia and central Europe. The long axes of the bars represent the maximum horizontal stress orientation and the length of the bar reflects the quality ranking of that indicator. Maximum horizontal stress is generally oriented ~NW-SE throughout much of Europe, though is more variable in the North Sea to the east of the British Isles. Note the paucity of stress orientations in the Faroe Shetland Region, with only four measurements included in the latest release of the World Stress Map database. This map also shows predicted maximum horizontal stress orientations based on the finite element analysis of Gölke & Coblentz (1996), which indicates uniform NW-SE compression throughout western Europe. World Stress Map data from Heidbach et al. (2008).

Figure 3

Geoseismic profiles across the Faroe-Shetland region showing the structural and stratigraphic setting of the continental margin between (a) the Møre Basin and the continent-ocean transition zone (modified after DECC Promote 2014), and (b) the

West Shetland margin and the Faroe-Shetland Basin (modified after Lamers & Carmichael, 1999). Inset map shows the bathymetry (x1000 m) of the NW European margin, location of the geoseismic profiles, and limit of map area in Figure 1. Other abbreviations: Ku, Upper Cretaceous; KL, Lower Cretaceous; J, Jurassic; PT, Permo-Triassic; SDRs, seaward-dipping reflectors.

Figure 4

(a) Results of a hollow cylinder laboratory test simulating borehole breakout (performed by the CSIRO Division of Geomechanics). The intersection of conjugate shear failure planes results in the enlargement and ovalization of the cross-sectional shape of the wellbore perpendicular to the orientation of σ_{Hmax}. (b) Examples of common types of enlarged boreholes (including breakouts) and their caliper log responses. . C1 is Caliper 1 which measures the diameter of the borehole between pads 1 and 3, and C2 is Caliper 2 which measures the diameter of the borehole between pads 2 and 4. The dashed circle represents the bit size, and the small filled circle represents the position of the sonde. This figure is from after Plumb & Hickman (1985) to which the reader is referred for further explanation. (c) Examples of borehole breakouts interpreted from four-arm caliper log data from well 205/21-1A in the SW stress province of the FSR.

Figure 5

Rose diagrams showing distribution of borehole breakouts (plotted as maximum horizontal stress orientations i.e. perpendicular to breakout orientation for the (a) SW stress province, (b) central stress province and (c) NE stress province. (d) shows breakout data from all 16 wells aggregated in one diagram.

Figure 6

(a) Schematic plan view diagram illustrating how maximum horizontal stress orientations can be deflected due to lateral variations in the elastic properties of rocks. In this case, stress trajectories encounter a zone that is relatively harder or stiffer that the surrounding rocks (e.g. a strong fault), causing deflections such that σ_{Hmax} intersects the interface between the zones of contrasting rock properties at right angles. (b) In this case, a 'softer' zone embedded within relatively harder rocks (e.g. a weak fault) causes σ_{Hmax} orientations to align parallel to the relatively weak or soft material. (a) and (b) Modified after Bell (1996) and Morley (2010). (c) Highly simplified block model proposed to account for aspects of the observed variation of σ_{Hmax} orientations within the FSR. In the NE of the region, where the rift-basin structural configuration is less complicated and the thickness of syn- and post-rift sediment is thicker, σ_{Hmax} orientations are consistent with those in adjacent regions and are interpreted to be controlled by a combination of plate-boundary forces and regional-scale source of stress (e.g. deglaciation-induced lithospheric flexure). In the SE of the region, weak basement-bounding faults cause local-scale deflections of σ_{Hmax} orientations.

844 **Table 1. Summary of breakouts in each well.**

845

Well	N	Number-Weighted		Length-Weighted			Quality
		Mean (°)	SD (°)	Mean (°)	SD (°)	Total Length (m)	
202/3A-3	6	64	13.9	58	17.4	98.5	C
202/9-1	4	43	17.0	42	15.4	156.0	C
204/28-1	15	171	22.2	158	21.5	81.0	C
205/10-2B	18	83	23.2	75	20.6	190.4	C
205/20-1	4	1	35.3	3	21.4	70.2	C
205/21-1A	24	95	10.9	91	10.0	247.4	B
206/3-1	1	35	-	35	-	125.9	D
206/5-1	18	67	23.6	69	17.9	548.0	B
206/8-5	15	125	17.4	122	14.2	66.7	C
208/26-1	17	117	46.6	109	33.7	520.7	D
209/3-1A	14	119	16.6	126	17.7	213.4	B
210/4-1	12	104	53.7	174	52.8	176.5	D
214/27-1	8	16	22.7	2	13.6	349.7	B
214/28-1	20	115	22.5	110	2291	88.8	C
214/29-1	18	37	34.9	42	26.9	240.3	D
219/20-1	8	138	30.4	154	18.7	66.1	C

846

Holford et al Figure 1

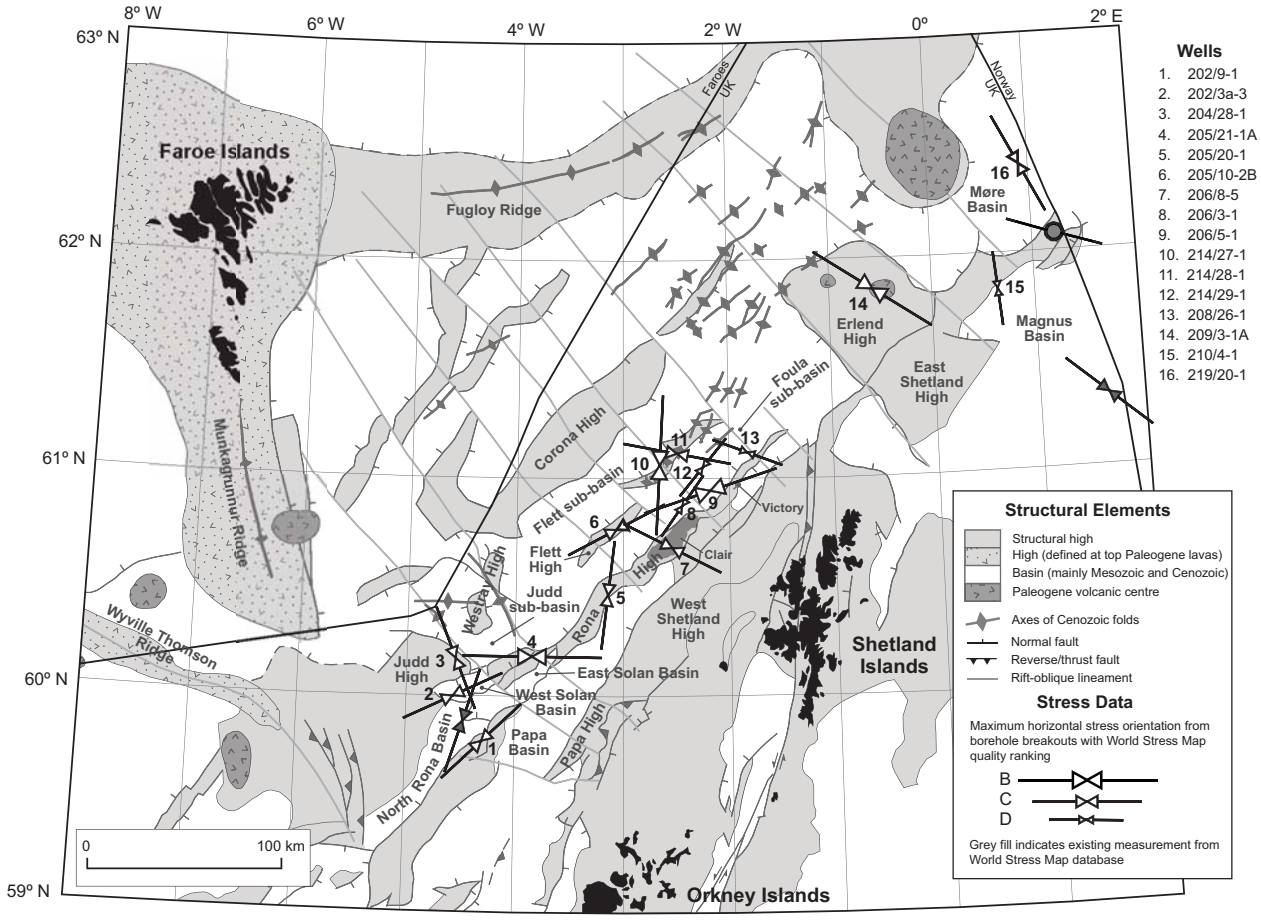

Holford et al Figure 2

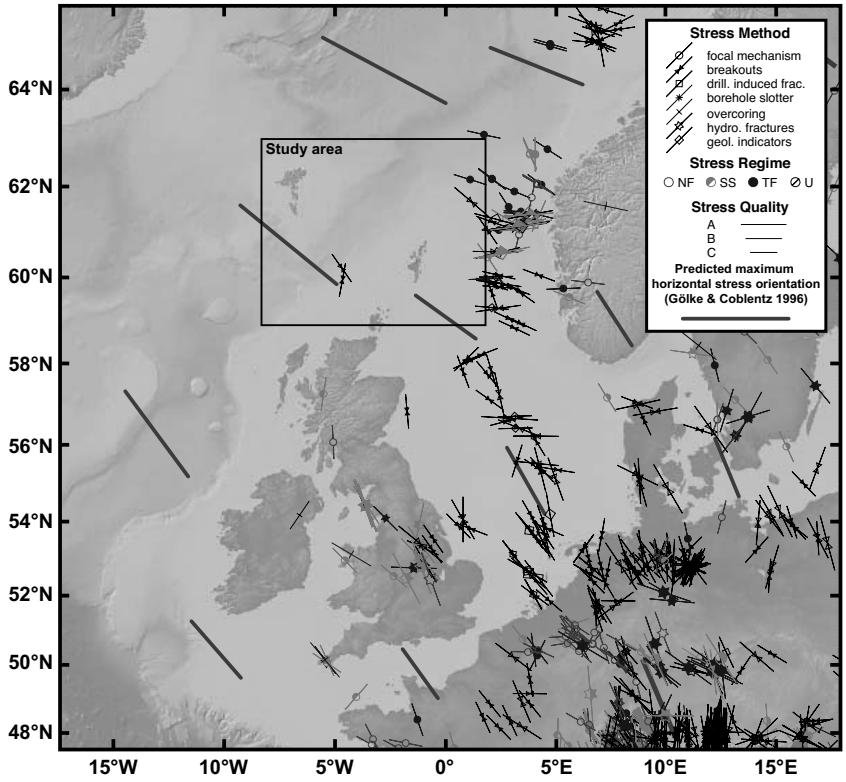

Holford et al Figure 3

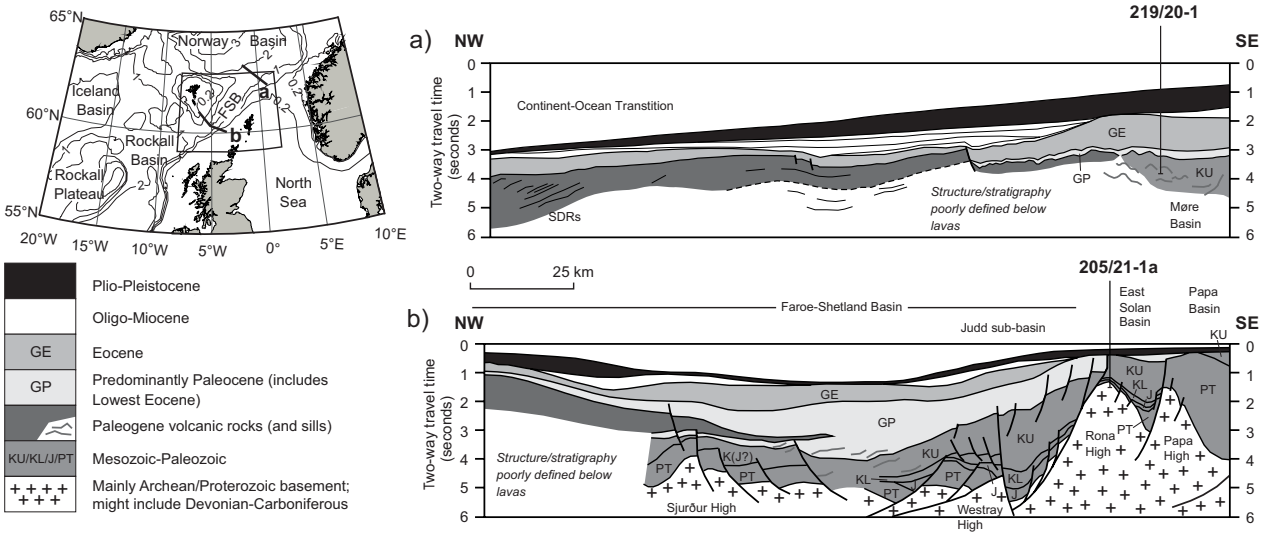

Holford et al Figure 4

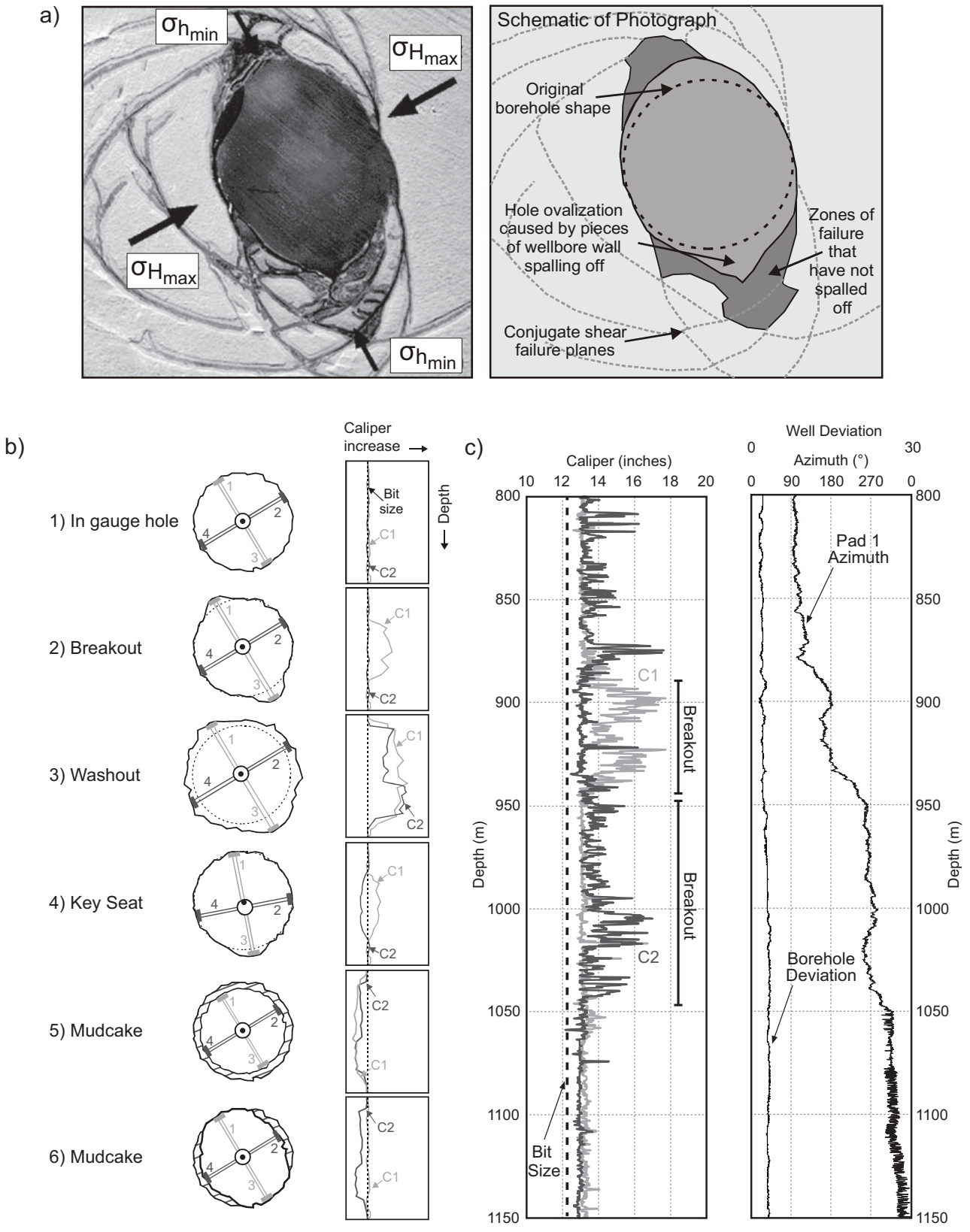

Holford et al Figure 5

a) SW province
202/9-1, 202/3a-3,
204/28-1, 205/21-1A

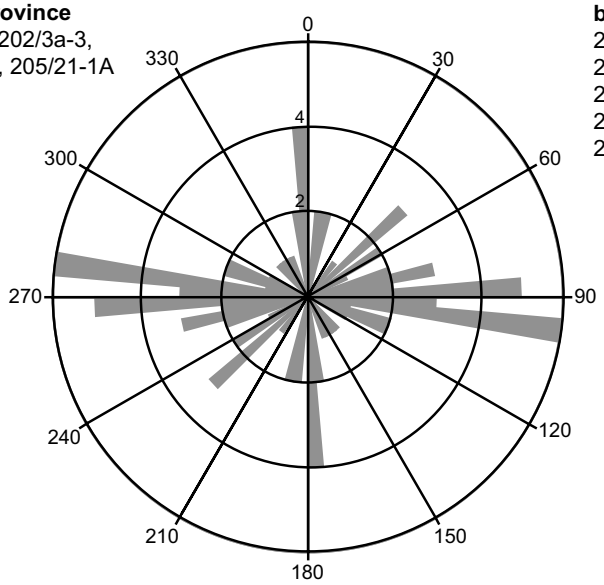

b) Central province
205/10-2B, 205/20-1,
206/3-1, 206/5-1,
206/8-5, 208/26-1,
214/27-1, 214/28-1,
214/29-1

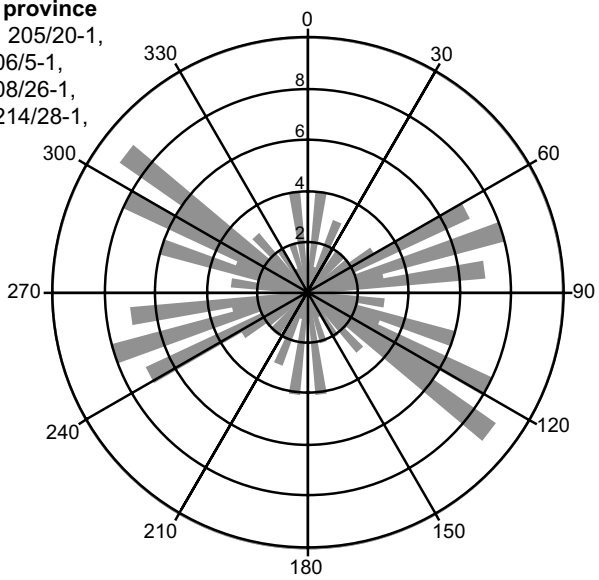

c) NE province
209/3-1A, 210/04-1,
219/20-1

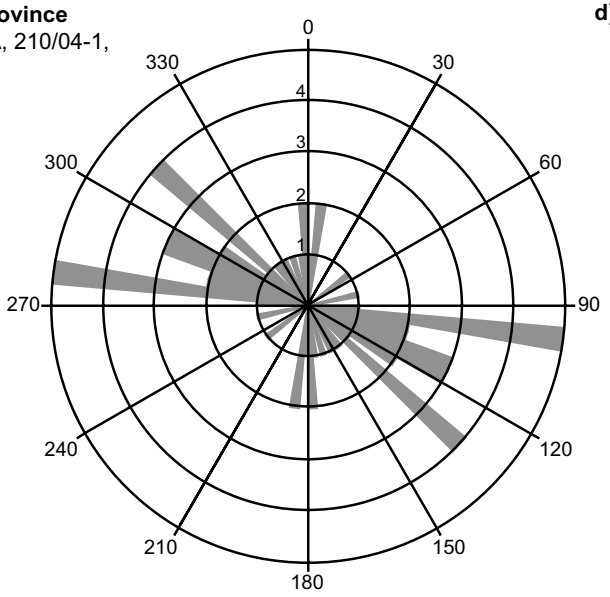

d) All data

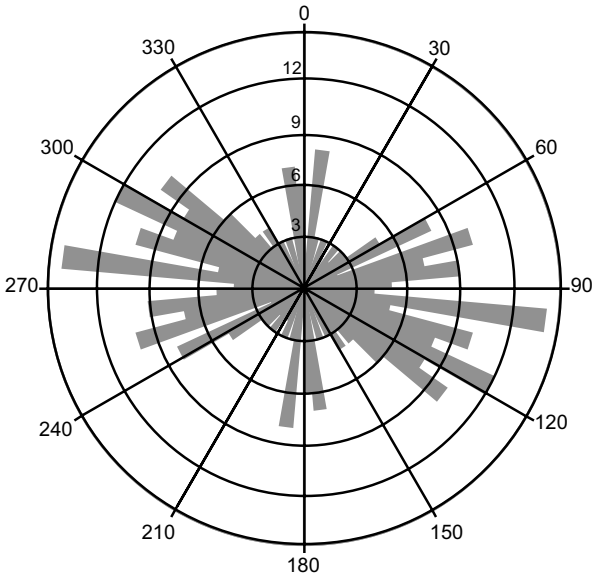

Holford et al Figure 6